Chemical Papers (2023) 77:5047–5057
https://doi.org/10.1007/s11696-023-02842-z

ORIGINAL PAPER

Comparison of structure and solar-selective absorbance properties of Al_2O_3 thin films with Al and Ni reflector interlayers

Aliaa Abdelfatah[1] · **Lamiaa Z. Mohamed**[1] · **Iman Elmahallawi**[1,2] · **Hanan Abd El-Fattah**[3]

Received: 2 March 2023 / Accepted: 20 April 2023 / Published online: 3 May 2023

Abstract

This work aims at evaluating the selective solar absorbance (SSA) of Al_2O_3 thin films deposited by physical vapor deposition (PVD) with two different metallic reflector interlayers. Al_2O_3 thin films are deposited on the same substrate stainless steel (SS) 304L, with two different interlayers between the thin film and the substrate, namely, nickel (Ni) and aluminum (Al) are used as the reflector interlayer SS304L/Al/Al_2O_3 and SS304L/Ni/Al_2O_3. A scanning electron microscope (SEM) was utilized to characterize the chemical composition by energy dispersive X-ray analysis (EDX) and surface morphology of the deposited thin films. The phases of the thin films were analyzed and identified by X-ray diffraction (XRD) to detect the present phases. The surface topography and the thickness of the deposited thin films were investigated using an atomic force microscope (AFM). The optical properties of the substrate and the deposited thin films (absorbance & emittance) in two conditions were identified by Fourier transform infrared spectroscopy (FTIR) and spectrophotometer. The obtained results demonstrate that both SS304L/Al/Al_2O_3 and SS304L/Ni/Al_2O_3 show good performance, such as high solar absorbance and low thermal emittance. However, the Al/Al_2O_3 thin film provides high selectivity (absorbance/emittance (α/ε)) of 0.916/0.05, compared to 0.913/0.15 for the Ni/Al_2O_3 coating. The effect of different properties and microstructure on the efficiency of deposited thin films showed that the SS304L/Al/Al_2O_3 has higher absorbance (92%) in visible and ultraviolet (UV) regions; and lower emittance (5%) than the SS304L/Ni/Al_2O_3. This work shows that the intermediate IR layer has a more pronounced effect on the emittance properties rather than the absorbance properties of the Al/Al_2O_3 layer.

Keywords Selective solar absorber · Solar thermal energy · Magnetron sputtering · SS304L substrate · Optical properties · Microstructure

Introduction

In line with current adopted strategies for integrating higher shares of renewable energy in the energy mix, solar energy utilization is expected to rise significantly to reduce the use of fossil energy (Singh et al. 2019; Rezvani et al. 2018; Ghahramanpour et al. 2020). Solar thermal energy stations transforming solar energy into electricity are expected to increase in countries in the sun-belt regions. Among the main functional parts of this system is the absorber. To improve heat transfer and selective absorptivity, the absorber should be coated. Through the focus on solar radiation, the coating should remain structurally and chemically stable at operating temperature (Wang et al. 2019a, 2019b). Thermal solar selective coatings with specific properties are deposited on metallic tubes and their performance is evaluated by their function as solar selective absorbers (SSA) with high absorbance in the light visible range and low emittance in the ultraviolet (UV) range (Zhang et al. 2020; Rebouta et al. 2015). Physical vapor deposition (PVD) and chemical vapor deposition (CVD) are widely adopted in recent years (Ryan et al. 1999). The PVD encompasses a wide range of vacuum deposition techniques. PVD employs physical processes such as sputtering and evaporation to generate a vapor of atoms, molecules, or ions from a target of the coating

✉ Lamiaa Z. Mohamed
lamiaa.zaky@cu.edu.eg

1 Mining, Petroleum, and Metallurgical Engineering Department, Faculty of Engineering, Cairo University, Giza, Egypt

2 The Centre for Renewable Energy, The British University in Egypt, El Shorouk, Cairo, Egypt

3 Department of Manufacturing Engineering and Production Technology, Modern Academy for Engineering and Technology, Cairo, Egypt

material to be deposited on the substrate surface as a coating (Pan et al. 2012; Baptista et al. 2018).

Heat is harvested by selective solar absorbers. At the operational temperature, the selective solar coating (SSC) should be both structurally and chemically stable (Mrkvica et al. 2022). As a result, obtaining maximum absorption on a single layer of coating is challenging. Depending on absorption mechanisms and design concepts, five types of selective solar absorbers are classified: (1) intrinsic absorber, (2) semiconductor metal, (3) multilayer interference stacks, (4) cermet absorber, (5) textured surface (Al-Rabeeah et al. 2022). Many factors influence light absorption, including the electronic structure wavelengths of the materials and specific surface features such as pits, peaks, or voids (Sandá et al. 2019). An anti-reflective layer, a metallic layer, an infrared reflector coating layer, and a dielectric layer are all alternate layers in multilayer absorbers (Al-Oran et al. 2020).

Stainless steel (SS) is the generic name for a wide range of metallic alloys that contain the main constituents Fe, C, Cr, Ni, and other transition elements (Lopez-Melendez et al. 2012) and are usually used for manufacturing absorber tubes in thermal solar systems. Compact thin films coatings were made with SS alloys prepared by magnetron sputtering (MS) (Burstein and Vines 2001; Yiu et al. 2021; Gateman et al. 2020), thermal spray coating (Xu et al. 2020), atomic layer deposition (Singh et al. 2019), ultrafast laser pulse, and cathodic arc ion plating (Nastulyavichus et al. 2020; Wang et al. 2021), or selective laser melting (SLM) (Wang et al. 2019b), to achieve solar selective absorbers (SSA).

Because metals are excellent conductive materials, using them as selective absorbers appears to be advantageous. Metals, while good absorbers, have a large emittance and therefore cannot be used in their metallic form, instead using they as oxides and nitrides (Abd El-Fattah et al. 2019a). Ti, Al Oxides, and Nitrides are increasing in popularity because of their important optical characteristics; additionally, they can be generated directly via sputtering or oxidation. Due to their high absorbance visible range of light at high temperatures and thermal stability, TiO_2, TiNOx, Al_2O_3, and AlN have been demonstrated to have great selective absorber properties (Abd El-Fattah et al. 2019b). To accelerate propagation to the absorber surface, an anti-reflective layer is deposited on the upper coating, and reflective material is used for the bottom layer (Wang et al. 2022). Many dielectric-metal interference stack multilayers are made of numerous dielectrics such as SiO_2, Al_2O_3, AlN, and others. Metals such as Ti, Al, Cu, Cr, Mo, Ni, and others are also used (Zou et al. 2017). The drawback of these stack coatings is that they are expensive to manufacture. Wet chemical methods have not gained popularity due to their failure at high temperatures (greater than 400 °C) (Abdulhamed et al. 2018; Suriwong et al. 2018). The possible explanation for this is that using a wet chemical method results in a coating with many structural problems, particularly in its density and purity. As a result, these drawbacks hinder the development of these coatings.

To reach optimal solar absorbance and low emissivity, the receiver tube is enveloped by selective solar coatings (Klocke and Krieg 1999). It has been shown that solar radiation is transformed into heat by the thickest Ni–Al coating (299 m) (Bobaru et al. 2022). The performance of the absorber coating layer deposited on the receiver controls the conversion of solar energy to heat. The AlNi/Al_2O_3 coating was reported to provide high selectivity (absorbance/ emittance (α/ε)) of 0.96/0.104 with high thermal stability (TS) at 600 °C in vacuum for 300 h (Al-Rabeeah et al. 2022). Al_2O_3 is used as a dielectric material in cermet coatings because of its low refractive index ($n = 1.65$) and high thermal stability. The maximum absorptance of 0.92 and minimum emittance of about 0.05 were noted in deposited multilayer thin films coated with the combination of tungsten, $Al_2O_{3,}$ and nickel, respectively. Xiudi et al. prepared a monolayer of Al_2O_3: Ag thin films by magnetron sputtering then annealed at 700 °C and 500 °C in the air several times. Different thicknesses and different annealing temperatures have been investigated (Xiao et al. 2012). After annealing at 500 °C for 70 h in air, the solar selectivity of multilayer films with absorbing layer thicknesses bigger than 120 nm did not deteriorate. Vijaya et al. (2018) deposited the Al_2O_3 layer by sputtering. Oxide thin film exhibits an enhancement to the optical properties of solar absorbers.

The main aim of this work is to further investigate the selective solar absorbance performance of Al_2O_3 deposited directly on the substrate, with an intermediate metal (Ni/ or Al), and to characterize the deposited thin films. The idea of this work is based on enhancing the thermal selective absorbance of the dielectric absorbing sublayer by inhibiting the diffusion of the constituent elements of the absorbing layer to the substrate during preparation and service conditions. Even though most of the researchers have investigated Ti oxides and Nitro oxides, previous work of the authors and others (Besisa et al. 2022; Zhou et al. 2022) has shown that Al_2O_3 is a challenging SSA, as it provides the lowest emittance but not the highest absorbance, the best thermal emissivity, the lowest thermal expansion, the most outstanding thermal shock resistance, and mechanical durability. Previous work has investigated different intermediate layers such as AlNi/Al_2O_3 and Ni/Al_2O_3 multilayer coatings (Al-Rabeeah et al. 2022; Xiao et al. 2012) and has shown enhancing selectivity properties through this strategy, but Al/Al_2O_3 coatings on SS substrates are not investigated in the literature. In this study, thin films of Al_2O_3 are deposited on SS304L substrates with an interlayer of Ni or Al in between, aiming at enhancing the absorptivity of the absorber tubes by adding a dual-purpose sub-reflector and diffusion barrier layer. Al and Ni are suggested as both having FCC structures, aiming at suppressing thermal diffusion between the substrate and the SS coating. While the atomic radius of Al is 0.143 nm compared to 0.124 nm for Ni, differences in diffusion are expected. The PVD method was used for the deposition. The morphological, structure analysis, absorbance, and emittance characteristics of the deposited Al_2O_3 are characterized. Also, the optical properties of the Al and Ni layers below the Al_2O_3 thin film were compared with each other.

Materials and methods

Selective solar coating (SSC) preparation

The deposition was done by sputtering at specified deposition conditions of two different multilayers. Al_2O_3 and Al/Ni thin films were deposited on SS304L substrates by PROTOFEEX sputtering 1600- Magnetron 6 (USA) sputtering tool at a frequency of 13.6 MHz and maximum output power of 2.5 kW. The chemical composition of SS304L is illustrated in Table 1. Pure Al target (99.999%), pure Ni target (99.999%), and pure Al_2O_3 target (99.999%) of size (30×10 cm^2) were utilized for the deposition of all thin films in the reactive medium using Ar gas at flow rate 30 Sccm. The SS substrates dimensions were 2×2 cm^2 with a thickness of 2 mm. Five substrates were put into the chamber for each run which was cleaned in acetone and isopropanol and then dried. They were fixed in the deposition chamber with a bias voltage equal to 150 V and 10 rpm rotation velocity. During the deposition, sputtering power was maintained at 1.15 kW, and the initial vacuum was 10^{-5} Pa but the chamber base pressure was pumped down to 10^{-3} Pa. The chamber (of a circular geometry with a diameter of 50 cm) was operated at a temperature reaching 160 °C during the sputtering process as recorded on the digital screen, and the distance between the target and the substrate was equal to 10 cm. The deposition time was 60 min for each layer. Figure 1 provides the schematic drawing of the solar selective absorber (SSA) layers design deposited on SS304L substrate (SS304L/Al/Al_2O_3–SS304L/Ni/Al_2O_3).

Thin films characterizations

Surface morphology

The surface morphology and cross section of the samples were observed by scanning electron microscope (SEM) (FEI inspect S-Netherlands) and energy dispersive X-ray analysis (EDX) (Bruker AXS-flash detector Germany). Mapping was used for identifying the elemental distribution in the surface and cross section of the deposited thin films. Also, an atomic force microscope (AFM) 5600LS AFM from Agilent Technologies was used for obtaining 2D and 3D AFM images for the morphological investigations. The deposited thin film thickness and total roughness were demonstrated by AFM.

Phase identification

Phase Identification was characterized using the X-ray diffraction (XRD) model Bruker with scanning range $10 \leq 2\theta \leq 100°$ intervals, step size 0.1°, and a Cu target operating at 40 kV and 30 mA. The average particle size of the coating was calculated using Debye–Scherer equation (given in Eq. (1)):

$$D = \frac{K\lambda}{\beta \cos\theta} \quad (1)$$

where "D" is the particle size, "k" is Scherer's constant ($K = 0.94$ for spherical shape), "λ" is the wavelength ($\lambda = 1.54056$ Å) of X-ray radiations, "β" is the width

Table 1 Chemical composition of SS304L in wt.%

Elements	C	Mn	P	S	Si	Cr	Ni	Fe
wt.%	0.018	1.53	0.03	0.03	0.50	18.20	8.04	Bal

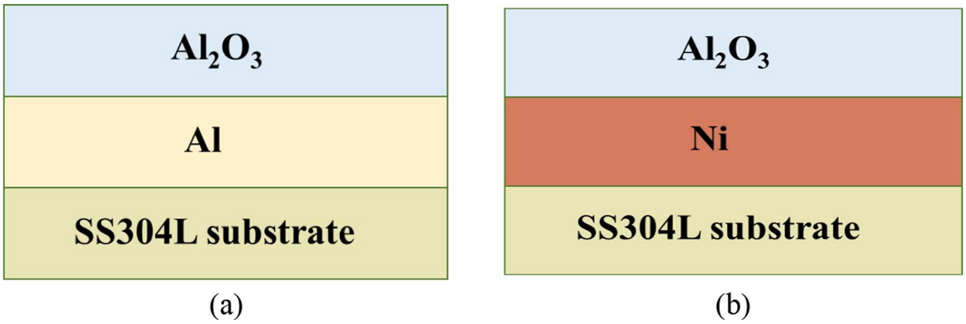

Fig. 1 SSA layers design

(full-width half maxima) of X-ray diffraction peak in radians and "θ" is the Bragg angle (Panigrahi et al. 2019).

Optical properties

The optical properties were characterized by using a spectrophotometer and Fourier transform infrared spectroscopy (FTIR) for absorbance and emittance, respectively. FTIR is NICOLET 6700 model. The spectrophotometer model is Shimadzu UV-3600. Absorbance characterization was in the ultraviolet (UV), visible, and near IR range (0.2–2.5 μm), while the emittance was measured in the long IR range (2.5–25 μm). The optical properties examination was made at room temperature. The determination of the desired properties from the test results was calculated on basis of Kirchhoff's law, stating that for opaque materials absorbance $\alpha(\lambda)$ and thermal emittance $\varepsilon(\lambda)$ are equal. The reflectance $R(\lambda)$ can be used to determine α & ε (Ollier et al. 2017) by Eq. (2):

$$\alpha(\lambda) = \varepsilon(\lambda) = 1 - R(\lambda) \tag{2}$$

The emittance $\varepsilon(T)$ at definite temperature T can be expressed by Eq. (3) (Zhou et al. 2022):

$$\varepsilon(T) = \frac{\int_{\lambda \min}^{\lambda \max} [1 - R(\lambda, T)]B(\lambda, T)\mathrm{d}\lambda}{\sigma T^4} \tag{3}$$

σ refers to Stefan–Boltzmann constant (5.6696×10^{-8} W m^{-2} K^{-4}).

B (λ, T) refers to blackbody spectral irradiance at λ and T. Planck's law is used to calculate B (λ & T) as shown in Eq. (4):

$$(\lambda, T) = \frac{C_1}{\lambda^5\left[e^{\left(\frac{C2}{\lambda T}\right)} - 1\right]} \tag{4}$$

Planck's first and second constants are $c1 = 3.7405 \times 10^8$ W μm^4 m^{-2} and $c2 = 1.43879 \times 10^4$ μm. K, respectively.

Results and discussion

Surface morphologies and composition of the coating

The SEM image of the SS304L substrate surface and the SS304L/Al/Al_2O_3 with their SEM mapping is shown in Fig. 2. The SEM surface morphology of the SS304L substrate shows a smooth and uniform coating layer all through as shown in Fig. 2b. The SEM mapping of the Al/Al_2O_3 thin film reveals the elemental distribution of the Al and O on the surface of SS304L showing their distribution over the surface. While Fig. 3 shows the SEM cross section of SS304L/Al/Al_2O_3 and SS304L/Ni/Al_2O_3 with their line EDX analysis. The line EDX analysis of SS304L/Al/Al_2O_3 shows the non-uniform distribution of the three elements Al, O, and Fe from the surface, inwards, while the line EDX analysis of SS304L/Ni/Al_2O_3 shows the uniform distribution of the three elements Al, O, and Ni. It can also be shown that the thin film of Ni/Al_2O_3 is more uniform, homogenous, and completely covers the substrate, as the Fe element is completely absent indicating that the SS substrate surface is fully coated by Ni. The non-uniform distribution at the beginning of Fig. 3b for Al is owed to its rise from two sources (Al metal intermediate and Al_2O_3 absorber layers) which leads to the non-uniformity of the reflected peaks. The same applies to the Ni as existed in Fig. 3d which also rises from both the intermediate layer and substrate. The chemical analysis of the SS304L substrate is shown in Table 1 which appears in line mapping of SS304L/Ni/Al_2O_3 (Cr & Ni). The strong Cr signal observed comes from the 304LSS substrate which has the highest percentage in stainless steel (about 18 wt.%). The Ni peak of the intermediate layer seems to combine with that from the substrate, and thus no significant Ni peak appears similar to that appearing in Fig. 3b for Al. The appearance of a small oxygen peak with Al and Ni at the beginning is owed to the absorber layer. Figure 4 shows the cross section elemental mapping for both SS304L/Al/Al_2O_3 and SS304L/Ni/Al_2O_3. The SEM stage performed initially has proved the deposition of the Al_2O_3 layers at the surface of the substrate for both Al and Ni substrates. However, the SEM study did not reveal much about the structure of the deposited layers. Similar observations were reported (Lazarov et al. 1992; Abd El-Fattah et al. 2020). Figure 4 shows the mapping of SS304L/Ni/Al_2O_3 which has a small layer of Al_2O_3than in the SS304L/Al/ Al_2O_3. The larger Al and O contents give more brightness at the surface of the cross section. However, the small amounts of Al and O give lower brightness at the surface of the cross section which appears in the colors throughout the cross section. This is not absolute but it is relative. Thus there is no Al and O throughout the cross section of SS304L/Ni/ Al_2O_3.

The surface morphology in 2D and 3D of SS304L and the as-deposited Al/Al_2O_3 and Ni/Al_2O_3 revealed by AFM are given in Fig. 5. The first column is 2D and the second column is 3D in Fig. 5. The Al_2O_3 film has good conformity and large area uniformity as shown in Fig. 5c. The size of the spherical shape crystallites for Al/Al_2O_3 is in the range of 10 ~ 35 nm, and about ~ 45 nm for Ni/Al_2O_3 (Vijaya et al. 2018). The total roughness of the surfaces of SS304L, SS304L/Al/Al_2O_3, and SS304L/Ni/Al_2O_3 are 21.5, 79.5, and 31.6 nm, respectively. The roughness of the coated surfaces increased after depositing thin films for both cases. Al/Al_2O_3 thin film shows the highest roughness

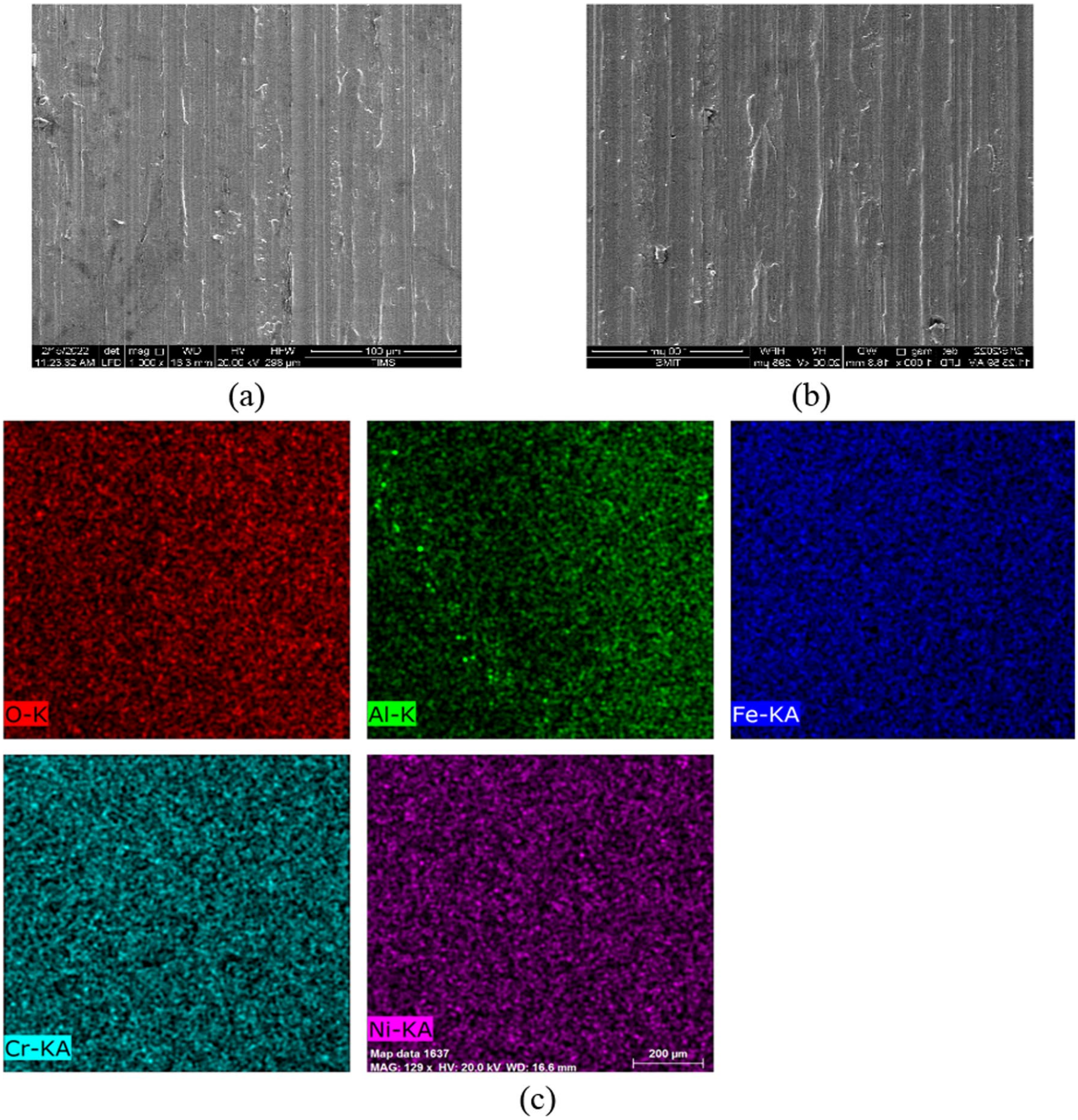

(a)

(b)

(c)

Fig. 2 SEM surface morphologies of **a** SS304L substrate, **b** SS304L/Al/Al_2O_3, and **c** elemental mapping of the coated surface of SS304L/Al/Al_2O_3

which leads to increasing the absorbance due to more scattering of the light in the thin film. Al/Al_2O_3 showed the highest absorbance as will be shown later in the optical properties section. Surface roughness rises during film growth due to the shadowing influence, which results from the preferential deposition of incident atoms on surface protrusions (Marin et al. 2013). The thickness of the deposited films of Al/Al_2O_3 and Ni/Al_2O_3 is 172 nm and 151 nm, respectively, which is appropriate for selective solar applications. As shown in Fig. 5b and c, depositing Al_2O_3 on the Al thin film leads to higher roughness compared to deposition on the Ni thin film.

Phase identification

The XRD was examined to study the phase identification of the substrate and the deposited thin films. Figure 6 shows the XRD results of the SS304L, SS304L/Al/Al_2O_3, and SS304L/Ni/Al_2O_3. The Al/Al_2O_3 shows diffraction peaks at 2θ values of Al 38.566°, 44.831°, 65.269°, and 78.444° (Pattern: COD 1512488) while 2θ values of Al_2O_3 (orthorhombic structure) are 38.527°, 40.527°, 41.670°, 44.777°, 65.127°, 77.222°, and 78.277° (Pattern: COD 1000442). The average particle size of Al_2O_3 calculated using the Debye–Scherer equation is 19 nm. The Ni/Al_2O_3 thin film shows diffraction peaks at 2θ values

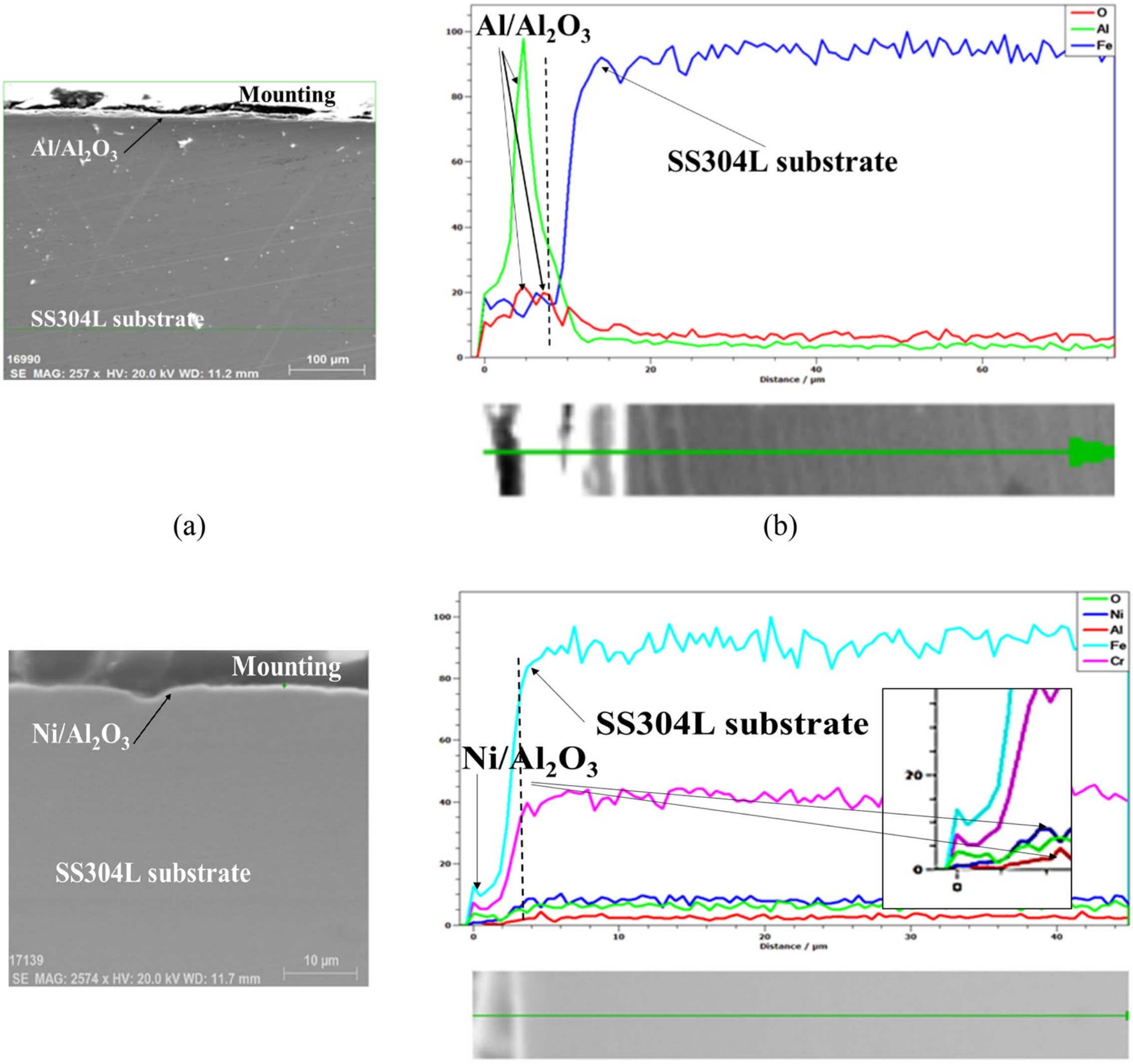

(a) (b)

(c) (d)

Fig. 3 SEM morphologies of the cross section of **a** SS304L/Al/Al_2O_3, and **c** SS304L/Ni/ Al_2O_3 and line EDX analyses for the cross section of **b** SS304L/Al/Al_2O_3 **d** and SS304L/Ni/Al_2O_3

at 44.215°, 51.518°, and 75.841° which belong to Ni (Pattern: COD 2100637) while 2θ values of Al_2O_3 (hexagonal structure) are 37.763°, 41.670°, 43.341°, 46.162°, 66.495°, and 77.222° (Pattern: COD 1000017) (Petrov et al. 2003; Abouarab et al. 2022; Qiang and Devarajan 2014). The SS substrate peaks are shown at 2θ values at 43.749°, 50.962°, and 74.948° (Pattern: COD 9014056) which belong to the solid solution of Iron (stainless steel) (Hänel et al. 2019).

The XRD results show that the Al_2O_3 deposited on the Al interlayer is the alpha form of the Al_2O_3 orthorhombic structure, while the oxide layer on the Ni interlayer is the alpha form of the Al_2O_3 hexagonal structure.

Optical properties

Figure 7 provides the absorbance of the SS304L substrate and the as-deposited thin films. The optical properties of the SS304L substrate are lower and different from the SS304L/Al/Al_2O_3 and SS304L/Ni/Al_2O_3 indicating that the measured optical properties reflect the morphological features of the coating and that the SS304L substrate did not interfere with the optical properties of the thin films. This is owed to the penetration of the reflected light beam of the spectrophotometer being of a limited traveling distance less than the thin film thickness (Abd El-Fattah et al. 2019a). The discontinuity in the absorbance curve

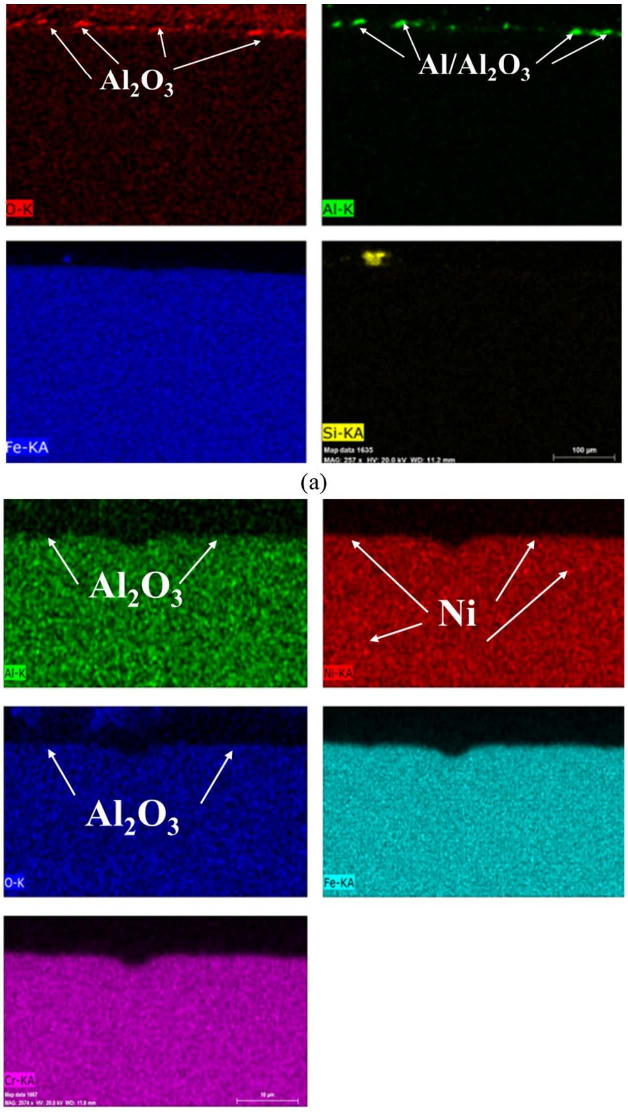

(a)

(b)

Fig. 4 Cross section elemental mapping of **a** SS304L/Al/Al_2O_3, and **b** SS304L/Ni/Al_2O_3

in the short IR range near 700–800 nm is not understood. It needs more investigation.

Figure 7 demonstrates that the as-deposited thin films show low reflectance (higher absorbance) in UV and visible light ranges and high IR reflectance (low absorbance). High absorbance in UV and visible regions is well known as a relatively steep edge, metal-like behavior. Interband transitions incorporating d-type free electrons are referred to as the relatively steep edge (Bonelli et al. 1992; Kennedy 2002). Also, Fig. 7 illustrates that Al/Al_2O_3 thin film has a higher absorbance. Figure 8 shows the emittance of the SS304L substrate and the as-deposited thin films.

The Al_2O_3 thin film deposited in this work on intermediate sublayers of Al/Al_2O_3 thin film provides high selectivity (absorbance/emittance (α/ε)) of 0.916/0.05. Similarly, it can be seen from the results that the absorbance/emittance (α/ε) for the Ni/Al_2O_3 deposited thin film is 0.913/0.15. The use of intermediate reflector sublayers has resulted in enhancement in lowering the emittance of the absorber layer. Careful selection of the reflector layer to consider its properties with relevance to not only reflectance but other properties affecting the total performance is important (Wang et al. 2022). In this study, the selection was made to consider diffusion properties that would affect the diffusion of some elements from the absorber layer to the substrate. In addition to its reflecting nature, the Al intermediate layer affected the surface roughness, and depositing Al_2O_3 on the Al thin film had higher roughness compared to deposition on the Ni thin film, which leads to increasing the absorbance due to more scattering of the light. The Al_2O_3 thin film deposited in this work, with spherical shape crystallites of size ranging from 19 nm (10 ~ 35 nm) for Al/Al_2O_3, and about ~ 45 nm for Ni/Al_2O_3 contributed to their selectivity performance. The crystallite sizes suggest that the Al_2O_3 thin film deposited in this work is α-Al_2O_3 type. Alpha and gamma alumina are two polymorphic structures of alumina. Alpha alumina has a low surface area and is almost non-porous, whereas gamma alumina has a high surface area with some porosity (Pajaczkowska et al. 2017).

The directly deposited α-Al_2O_3 in this work showed an absorbance of 0.916–0.913 and an emittance of 0.05–0.15, for Al/Al_2O_3 and Ni/Al_2O_3 coatings, respectively, with agglomerated grains compared to the as-deposited thin film. By comparing the emittance of the as-deposited thin films with oxidized films, the previous work by the authors (Abouarab et al. 2022) has shown that Al thin films oxidized at 400 °C showed an absorbance of 88% and an emittance of < 0.1. Oxidizing in the range of (400–800 °C) changed the morphology and Al thin film structure promoting the formation of α and γ-Al_2O_3. It was suggested that fibrous and rod-like structures are more beneficial to the optical properties of the SSAs. Accordingly, comparing the results obtained in this work and the previous one (Abouarab et al. 2022) shows some interesting observations. The Al_2O_3 formed in previous work by oxidizing Al at different temperatures (400–800 °C) showed a stable absorbance pattern in the range 88–90% in UV, visible, and short IR range, whereas the deposited Al_2O_3 in this work shows a steep absorbance pattern of 90% in UV range only with a decrease in the visible and short IR range. The higher and stable absorbance of the Al_2O_3 in useful light ranges is owed to the formed morphology after oxidation. This morphology has resulted from the low solubility of oxygen in Al segregates formed at grain boundaries GB and surfaces, so oxide layers were formed which extremely reduce GB mobilities and Al surface activity. Also, the oxidizing conditions favored the formation of stable nanoparticles, which agglomerate to cover the whole

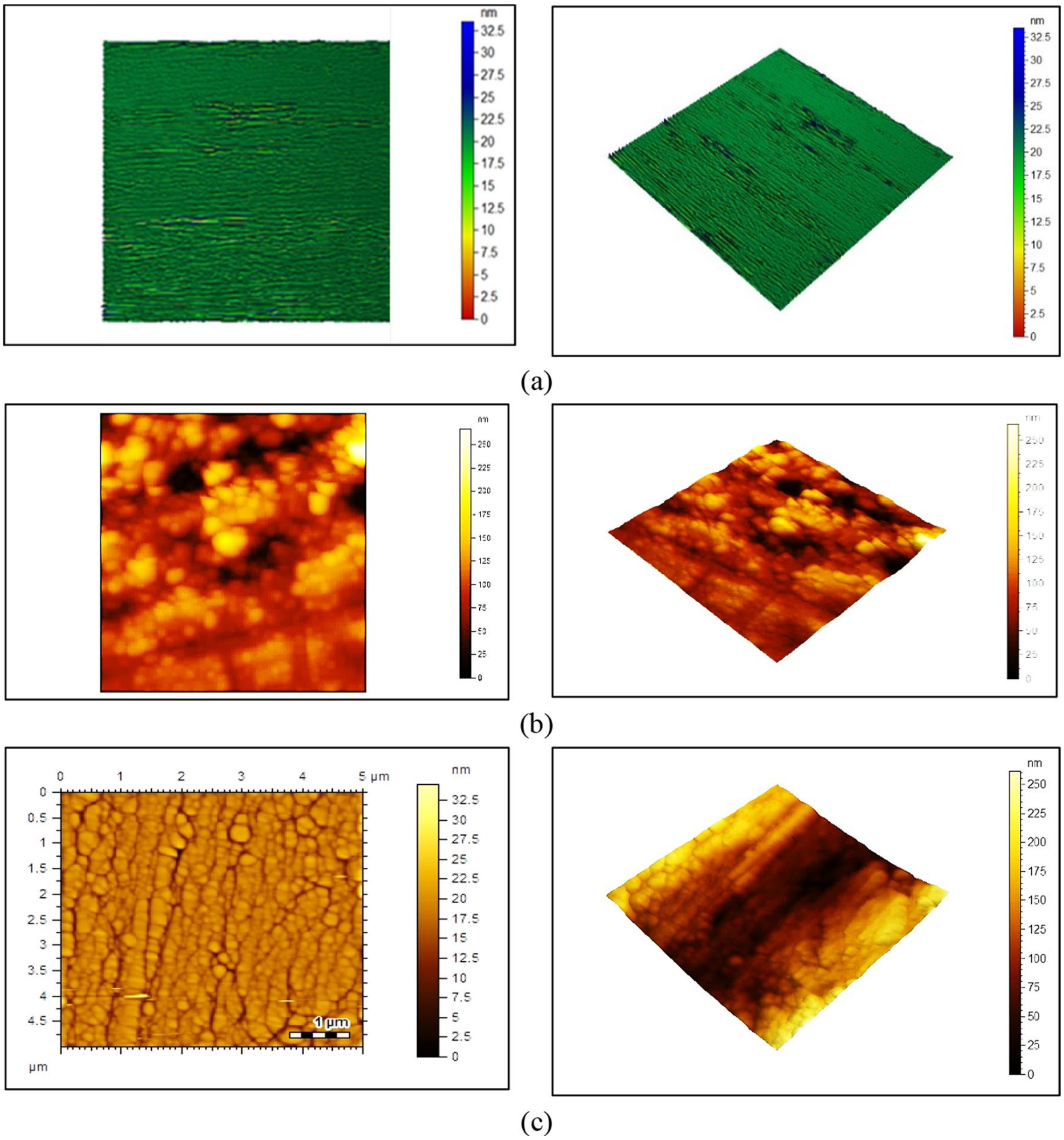

Fig. 5 AFM images 2D and 3D of **a** SS304L, **b** SS304L/Al/Al_2O_3, and **c** SS304L/Ni/Al_2O_3

surface. The γ- Al_2O_3 structure forming after oxidation in the range of (400–800 °C) consists of agglomerated grains of fibrous and rod-like structures. These structures result in enhanced optical properties suiting the requirements of high selective solar absorbers SSAs.

Conclusions

In this work, two intermediate layers are compared and evaluated as reflector layers for the Al_2O_3 absorber. The two investigated structures are SS304L/Al/Al_2O_3 and SS304L/Ni/Al_2O_3. Both SS304L/Al/Al_2O_3 and SS304L/Ni/Al_2O_3 deposited coatings exhibited relatively steep edge, metal-like behavior but the former showed slightly higher absorbance properties than the SS304L/Ni/Al_2O_3. The SS304L/Al/Al_2O_3 showed absorbance and selectivity (absorbance/emittance (α/ε)) of about 92% and 0.916/0.05, respectively. The SS304L/Ni/Al_2O_3 deposited coatings showed absorbance and selectivity (absorbance/ emittance (α/ε)) of about 91.3% and 0.913/0.15, respectively. The work has shown a slight effect of the intermediate layer on the absorbance properties of the Al_2O_3 layer, but a more pronounced effect is shown on the emittance as it changed from 0.15 to 0.05 when Al was used as the intermediate layer. This is owed to Al acting as a barrier to diffusion

Fig. 6 XRD patterns of SS304L substrate before coating, SS304L/Al/Al_2O_3, and SS304L/Ni/ Al_2O_3

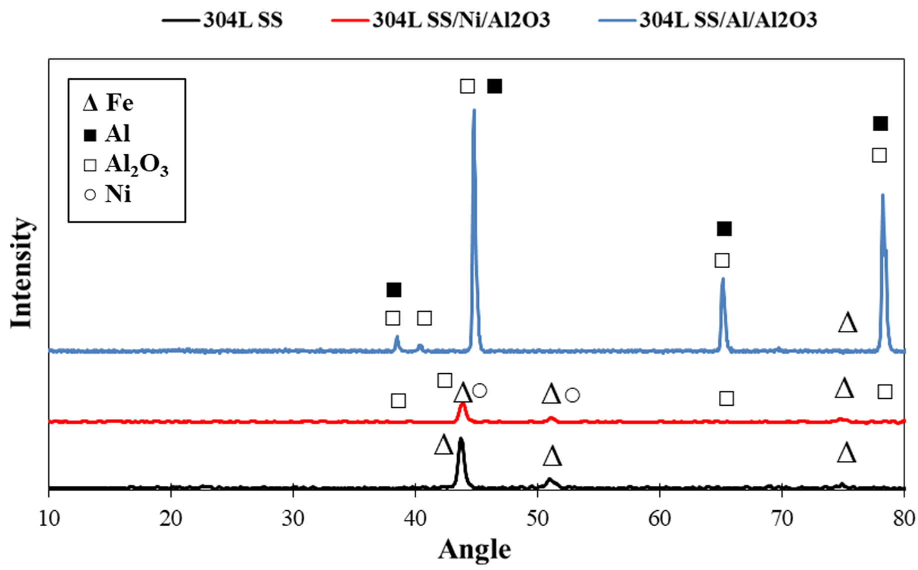

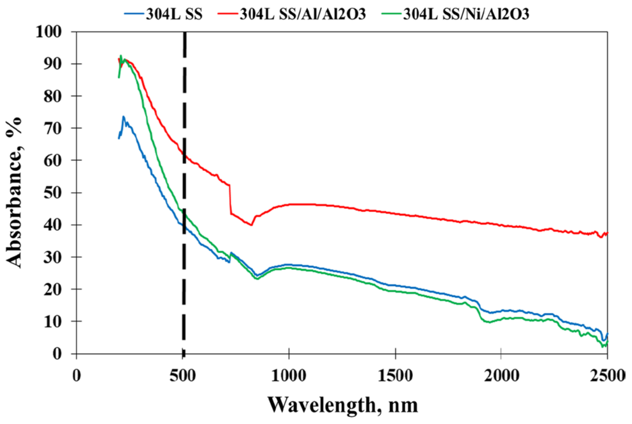

Fig. 7 Absorbance of SS304L, SS304L/Al/Al_2O_3, and SS304L/Ni/ Al_2O_3 in the visible range

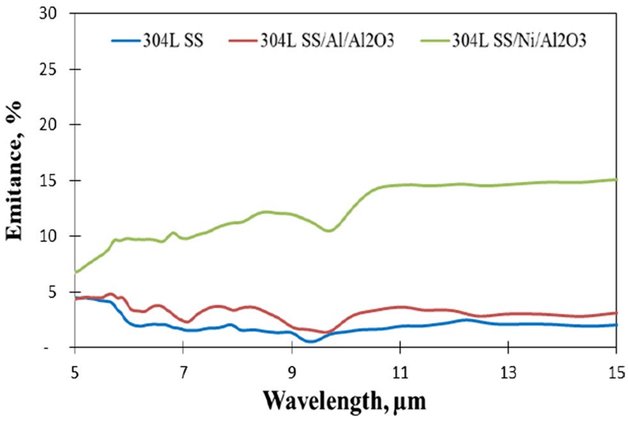

Fig. 8 Emittance of SS304L, SS304L/Al/Al_2O_3, and SS304L/Ni/ Al_2O_3 in UV range

of the absorbance layer into the substrate, in addition to its functioning as a reflector layer.

Acknowledgements The authors acknowledge Cairo University for their support.

Author Contributions Conceptualization contributed by AA, LM, IE, and HAEl-F; methodology contributed by AA, LM, IE, and HAEl-F; software contributed by AA, LM, IE, and HAEl-F; validation contributed by AA, LM, IE, and HAEl-F; formal analysis contributed by AA, LM, IE, and HAEl-F; investigation contributed by AA, LM, IE, and HAEl-F; resources contributed by AA, LM, IE, and HAEl-F; data curation contributed by AA, LM, IE, and HAEl-F; writing—original draft preparation contributed by AA, LM, IE, and HAEl-F; writing—review and editing contributed by AA, LM, IE, and HAEl-F; visualization contributed by AA, LM, IE, and HAEl-F; supervision contributed by AA, LM, IE, and HAEl-F; project administration contributed by AA, LM, IE, and HAEl-F; funding acquisition contributed by AA, LM, IE, and HAEl-F.

Funding Open access funding provided by The Science, Technology & Innovation Funding Authority (STDF) in cooperation with The Egyptian Knowledge Bank (EKB). This work is funded by Cairo University Research Support Program for Renewable Energy.

Data availability statement The data that support the findings of this study are available from the corresponding author upon reasonable request.

Declarations

Conflict of interest The authors declare that they have no conflicts of interest.

Ethical statement This article does not contain any studies involving animals performed by any of the authors. Also, it does not contain any studies involving human participants performed by any of the authors.

References

Abd El-Fattah H, El-Mahallawi I, Shazly M, Khalifa W (2019a) Optical properties and microstructure of TiNxOy and TiN thin films before and after annealing at different conditions. Coatings 9(1):22

Abd El-Fattah H, Shazly M, El-Mahallawi I, Khalifa W (2019b) Optical properties and microstructure of TiN Thin films before and after annealing. Mater Express 1(9):2158–5849

Abd El-Fattah HA, El-Mahallawi IS, Shazly MH, Khalifa WA (2020) Microstructure evolution of NiTi magnetron sputtered thin film on different substrates. Key Eng Mater 835:68–74

Abdulhamed AJ, Adam NM, Ab-Kadir MZA, Hairuddin AA (2018) Review of solar parabolic-trough collector geometrical and thermal analyses, performance, and applications. Renew Sustain Energy Rev 91:822–831

Abouarab H, El-Mahallawi I, Kassry A, Abd El-Fattah H (2022) Characteristics of Al & Ti oxide-thin films for thermal solar energy selective absorption applications. Mater Express 12:968–979

Al-Oran O, Lezsovits F, Aljawabrah A (2020) Exergy and energy amelioration for parabolic trough collector using mono and hybrid nanofluids. J Therm Anal Calorim 140(3):1579–1596

Al-Rabeeah AY, Seres I, Farkas I (2022) Selective absorber coatings and technological advancements in performance enhancement for parabolic trough solar collector. J Therm Sci 31:1990–2008

Baptista SF, Porteiro J, Míguez J, Pinto G (2018) Sputtering physical vapour deposition (PVD) coatings: a critical review on process improvement and market trend demands. Coatings 8:402

Besisa D, Ewais E, Mohamed H (2022) Thermal performance, and mechanical durability of Al_2O_3/CuO ceramics as solar receiver materials for solar thermal applications. Ceram Int 48(16):23609–23617

Bobaru S, Rico-Gavira V, García-Valenzuela A, Lopez-Santos C, Gonzalez-Elipe AR (2022) Electron beam evaporated versus magnetron sputtered nanocolumnar porous stainless steel: corrosion resistance, wetting behavior and anti-bacterial activity. Mater Today Commun 31:103266

Bonelli M, Guzman LA, Miotello A, Calliari L, Elena M, Ossi PM (1992) Structure and optical properties of TiN films prepared by dc sputtering and by ion beam assisted deposition. Vacuum 43(5–7):459–462

Burstein GT, Vines SP (2001) Repetitive nucleation of corrosion pits on stainless steel and the effects of surface roughness. J Electrochem Soc 148:B504–B516

Gateman SM, Page K, Halimi I, Nascimento ARCS, Savoie S, Schulz R, Moreau C, Parkin IP, Mauzeroll J (2020) Corrosion of one-step superhydrophobic stainless-steel thermal spray coatings. ACS Appl Mater Interfaces 12:1523–1532

Ghahramanpour M, Jamehbozorgi S, Rezvani M (2020) The effect of encapsulation of lithium atom on supramolecular triad complexes performance in solar cell by using theoretical approach. Adsorption 26:471–489

Hänel A, Janczarek M, Lieder M, Jan H (2019) Photocatalytic decomposition of air pollutants using electrodeposited photocatalysts on stainless steel. Pol J Environ Stud 28(3):1157–1164

Kennedy CE (2002) Review of Mid, to high-temperature solar selective absorber Materials. National Renewable Energy Laboratory, pp 520–31267

Klocke F, Krieg T (1999) Coated tools for metal cutting edge-features and applications. CIRP Ann Manuf Technol 48:515–525

Lazarov BM, Sizmann R, Goff AH, Granqvist CG, Lampert CM (1992) Calorimetric measurements of the total hemispherical emittance of selective surfaces at high temperatures. Proc SPIE 1727:149–161

Lopez-Melendez C, Bautista-Margulis RG, Garcia-Ochoa EM, EsparzaPonce HE, Carreno-Gallardo C, Gaona-Tiburcio C, Uruchurtu-Chavarin J, Villafane M (2012) Evaluation of corrosion resistance of thin films 304 stainless steel deposited by sputtering. Int J Electrochem Sci 7:1149–1159

Marin E, Lanzutti A, Fedrizzi L (2013) Tribological properties of nanometric atomic layer depositions applied on AISI 420 stainless steel. Tribol Ind 35(3):208–216

Mrkvica I, Szotkowski T, Slaninkova A, Jurga T (2022) High-efficiency of PVD coating process by applying an additional rotation. Coatings 12:834

Nastulyavichus AA, Kudryashov SI, Saraeva IN, Smirnov NA, Rudenko AA, Tolordava ER, Zayarny DA, Gonchukov SA, Ionin AA (2020) Nanostructured steel for antibacterial applications. Laser Phys Lett 17:6

Ollier E, Dunoyer N, Szambolics H, Lorin G (2017) Nanostructured thin films for solar selective absorbers and infrared selective emitters. Sol Energy Mater Sol Cells 170:205–210

Pajaczkowska PA, Reiche P, Klimm D, Majumdar G (2017) MgO, $MgAl_2O_4$, α-Al_2O_3, $LiAlO_2$, $LiGaO_2$, $NdGaO_3$, and $SrLaGaO_4$: bulk growth. In: Reference module in materials science and materials engineering

Pan C, Liu L, Zhang YB, Wang FH (2012) The electrochemical corrosion behaviour of nanocrystalline 304 stainless steel prepared by magnetron sputtering. J Electrochem Soc 159:C453–C460

Panigrahi UK, Das PK, Babu PD, Mishra NC, Mallick P (2019) Structural, optical and magnetic properties of Ni−xZnxO/Ni nanocomposite, Springer Nature Switzerland AG.

Petrov I, Barna P, Hultman L, Greene J (2003) Microstructural evolution during film growth. J Vac Sci Technol A 21:S117–S128

Qiang LW, Devarajan M (2014) Variation of structural and surface properties of RF sputtered aluminum oxide (Al_2O_3) thin films due to the influence of annealing temperature and time. Int J Mater Sci Appl 3(6):404–409

Rebouta L, Sousa A, Capela P, Andritschky M, Santilli P, Matilainen A, Pischow K, Barradas NP, Alves E (2015) Solar selective absorbers based on Al_2O_3: W cermets and AlSiN/AlSiON layers. Sol Energy Mater Sol Cells 137:93–100

Rezvani M, Ganji S, Jameh-Bozorghi S, Niazi A (2018) DFT/TD-semiempirical study on the structural and electronic properties and absorption spectra of supramolecular fullerene-porphyrine-metalloporphyrine triads based dye-sensitized solar cells. Spectrochim Acta A Mol Biomol Spectrosc 5(194):57–66

Ryan MP, Laycock NJ, Isaacs HS, Newman RC (1999) Corrosion pits in thin films of stainless steel. J Electrochem Soc 146:91–97

Sandá A, Moya SL, Valenzuela L (2019) Modelling and simulation tools for direct steam generation in parabolic-trough solar collectors: a review. Renew Sustain Energy Rev 113:109226

Singh AK, Adstedt K, Brown B, Singh PM, Graham S (2019) Development of ALD coatings for harsh environment applications. ACS Appl Mater Interfaces 11:7498–7509

Suriwong T, Bunmephiphit C, Wamae W, Banthuek S (2018) Influence of Ni–Al coating thickness on spectral selectivity and thermal performance of parabolic trough collector. Mater Renew Sustain Energy 7(3):1–9

Vijaya G, Singh M, Krupashankara MS, Srinivas MR, Kulkarni RS (2018) Development and analysis of tungsten-aluminium oxide based solar thermal multilayer coating. Mater Today Proc 5:2547–2554

Wang Z, Paschalidou E-M, Seyeux ZS, Maurice V, Marcus P (2019a) Mechanisms of Cr and Mo enrichments in the passive oxide film on 316L austenitic stainless steel. Front Mater 6:232

Wang ZW, Shen LD, Qiu MB, Jiang W, Chen Y, Zhao JF (2019b) Study on the properties of superhydrophobic coating prepared by scanning electrodeposition on SLM substrate. Mater Res Express 6:10

Wang X, Yuan X, Gong D, Cheng X, Li K (2021) Optical properties and thermal stability of AlCrON-based multilayer solar selective absorbing coating for high temperature applications. J Mater Res Technol 15:6162–6174

Wang X, Kang Y, Yuan X, Gong D, Li K (2022) A feasible and promising strategy for improving the solar selectivity and thermal stability of cermet-based photo thermal conversion coatings. Materials 15:6847

Xiao X, Xu G, Xiong B (2012) The film thickness dependent thermal stability of Al_2O_3: Ag thin films as high-temperature solar selective absorbers. J Nanopart Res 14:746

Xu K, Du M, Hao L, Mi J, Yu Q, Li S (2020) A review of high-temperature selective absorbing coatings for solar thermal applications. J Materiomics 6:167–182

Yiu P, You JD, Wang ST, Chu JP (2021) Tunable hydrophilicity in a surface nanotextured stainless steel thin film deposited by DC magnetron sputtering. Appl Surf Sci 555:149705

Zhang J, Wang C, Shi J, Wei D, Zhao H, Ma C (2020) Solar selective absorber for emerging sustainable applications. Adv Energy Sustain Res 3:2100195

Zhou J, Li S, Yu Y (2022) First principle calculation of thermal conversion properties of W-Al_2O_3 based solar selective absorbing coating. Comput Mater Sci 211:111501

Zou B, Dong J, Yao Y, Jiang Y (2017) A detailed study on the optical performance of parabolic trough solar collectors with Monte Carlo Ray Tracing method based on theoretical analysis. Sol Energy 147:189–201